Published in final edited form as:
J Biomech Eng. 2008 December ; 130(6): 061003. doi:10.1115/1.2979872.

Numerical Approximation of Tangent Moduli for Finite Element Implementations of Nonlinear Hyperelastic Material Models

Wei Sun[1],
Department of Mechanical Engineering, University of Connecticut, Storrs, CT 06269

Elliot L. Chaikof, and
Department of Surgery, and Department of Biomedical Engineering, Emory University and Georgia Institute of Technology, Atlanta, GA

Marc E. Levenston
Department of Mechanical Engineering, Stanford University, Stanford, CA

Wei Sun: weisun@engr.uconn.edu; Elliot L. Chaikof: ; Marc E. Levenston:

Abstract

Finite element (FE) implementations of nearly incompressible material models often employ decoupled numerical treatments of the dilatational and deviatoric parts of the deformation gradient. This treatment allows the dilatational stiffness to be handled separately to alleviate ill conditioning of the tangent stiffness matrix. However, this can lead to complex formulations of the material tangent moduli that can be difficult to implement or may require custom FE codes, thus limiting their general use. Here we present an approach, based on work by Miehe (Miehe, 1996, "Numerical Computation of Algorithmic (Consistent) Tangent Moduli in Large Strain Computational Inelasticity," Comput. Methods Appl. Mech. Eng., 134, pp. 223–240), for an efficient numerical approximation of the tangent moduli that can be easily implemented within commercial FE codes. By perturbing the deformation gradient, the material tangent moduli from the Jaumann rate of the Kirchhoff stress are accurately approximated by a forward difference of the associated Kirchhoff stresses. The merit of this approach is that it produces a concise mathematical formulation that is not dependent on any particular material model. Consequently, once the approximation method is coded in a subroutine, it can be used for other hyperelastic material models with no modification. The implementation and accuracy of this approach is first demonstrated with a simple neo-Hookean material. Subsequently, a fiber-reinforced structural model is applied to analyze the pressure-diameter curve during blood vessel inflation. Implementation of this approach will facilitate the incorporation of novel hyperelastic material models for a soft tissue behavior into commercial FE software.

Introduction

Numerical simulation of the nonlinear anisotropic mechanical behaviors of soft tissues and structured biomaterials remains an important and challenging topic in computational biomechanics. Various nonlinear strain energy functions have been developed for soft tissues, including those assuming material isotropy [1,2], transverse isotropy [3–6], orthotropy [7–12], and structural constitutive models involving invariants related to fiber organization [13–16]. While most constitutive modeling efforts are focused on the characterization of tissue behavior from experimental data, actual computational applications utilizing these

1Corresponding author. Also at Biomedical Engineering, 203 Bronwell Building, University of Connecticut, Storrs, CT 06269-3139.

experimentally driven user defined constitutive models have been rather limited. Moreover, the development and validation of new constitutive models are often conducted using custom finite element (FE) codes, and the difficulty of implementing such models within commercial FE codes poses a practical obstacle to their wide-spread application.

To implement a constitutive model into a commercial FE code such as ABAQUS (Version 6.5, Pawtucket, RI), the Cauchy stress tensor and the tangent modulus tensor (also referred to as the material Jacobian) derived from the constitutive model need to be explicitly specified. The tangent moduli (components of the tangent modulus tensor) serve as an iterative operator for an implicit FE solver using a Newton-type method for the solution of nonlinear initial boundary-value problems. Even though an exact closed-form solution for the tangent moduli gives the most rapid convergence, the exact tangent moduli are not mandatory to achieve accurate solutions. For highly nonlinear materials including soft tissues that exhibit "strain-stiffening" J-shaped stress-strain curves, however, approximations of the tangent moduli should be close to the true value to avoid numerical convergence issues.

Many soft tissues are commonly assumed to be incompressible or nearly incompressible at physiological loading rates. To model such materials, a decoupled representation of dilatational (volumetric) and deviatoric (isochoric) deformations is often employed. This treatment allows the dilatational stiffness be handled separately, allowing ill conditioning of the tangent stiffness matrix to be treated by numerical techniques [6]. However, such a treatment may lead to a mathematically complex formulation of the tangent stiffness matrix, and implementation as a user material subroutine in a FE code requires considerable algebraic manipulation and is prone to coding errors. A robust technique for an accurate numerical approximation of the tangent moduli that can be easily implemented for arbitrary strain energy formulations would therefore be an attractive alternative.

In this study we present an approach based on the work of Miehe [17] to numerically approximate the tangent modulus for a hyperelastic material model within the commercial FE platform ABAQUS. By incrementally perturbing the deformation gradient, the tangent moduli from the Jaumann rate of the Kirchhoff stress are approximated by a forward difference of the associated Kirchhoff stresses. We present an initial validation using a neo-Hookean material model and a subsequent numerical example of the approximation method in the context of a fiber-reinforced hyperelastic material model for blood vessels.

Method

Kinematics

Let Ω_0 and Ω be the (fixed) reference and deformed configurations of the continuous body, respectively. We consider the general mapping $\chi:\Omega_0\rightarrow\mathbb{R}^3$, which transforms a material point $X\in\Omega_0$ to a position $x=\chi(X, t)\in\Omega$ in the deformed configuration at time t. The deformation gradient tensor $\mathbf{F}$ is defined as $\mathbf{F}(X, t)=\partial\chi(X, t)/\partial X$. The spatial velocity field may be expressed as $\upsilon(x, t)=\partial x/\partial t$. The spatial velocity gradient $\mathbf{L}$ is defined as the derivative of a spatial velocity field with respect to the spatial coordinates $\mathbf{L}(x, t)=\partial\upsilon(x, t)/\partial x=\dot{\mathbf{F}}\mathbf{F}^{-1}$. Furthermore, let J=det $\mathbf{F}$ be the Jacobian of the deformation, where $J-1$ is a measure of the volumetric strain.

The symmetric and positive definite right and left Cauchy–Green tensors are defined as $\mathbf{C}=\mathbf{F}^T\mathbf{F}$ and $\mathbf{b}=\mathbf{F}\mathbf{F}^T$, respectively. For computational convenience, a multiplicative decomposition of the deformation gradient $\mathbf{F}$ is usually performed. Here, $\mathbf{F}$ is decomposed into a volumetric part $\mathbf{F}^{\sim}=J^{1/3}\mathbf{I}$ and a deviatoric part $\mathbf{F}^{-}=J^{-1/3}\mathbf{F}$. Consequently, the deviatoric right and left Cauchy–Green strain tensors $\mathbf{C}^{-}$ and $\mathbf{b}^{-}$ are defined as $\mathbf{C}^{-}=\mathbf{F}^{-T}\mathbf{F}^{-}$ and $\mathbf{b}^{-}=\mathbf{F}^{-}\mathbf{F}^{-T}$, respectively.

Stress Measures

In nonlinear problems, various stress measures can be defined. Three measures of stress are considered here: the second Piola–Kirchhoff stress, **S**, the Cauchy stress, σ, and the Kirchhoff stress, τ For hyperelastic materials, a scalar-valued strain-energy function ψ=ψ(**F**) is postulated to exist, allowing the second Piola–Kirchhoff stress **S**, Cauchy stress σ, and Kirchhoff stress τ to be derived as

$$\mathbf{S}=2\frac{\partial\psi}{\partial\mathbf{C}},\quad \boldsymbol{\sigma}=\frac{2}{J}\mathbf{F}\frac{\partial\psi}{\partial\mathbf{C}}\mathbf{F}^{T},\quad \boldsymbol{\tau}=J\boldsymbol{\sigma} \tag{1}$$

In finite element procedures, the Cauchy and Kirchhoff stresses are associated with updated Lagrangian formulations, whereas the second Piola–Kirchhoff stress is associated with total Lagrangian formulations [18]. Although the total and updated Lagrangian formulations are superficially quite different, the underlying mechanics of the two formulations are identical. Expressions in the total Lagrangian formulation can be transformed to updated Lagrangian expressions and vice versa. For example, the second Piola–Kirchhoff stress can be transformed to the Cauchy stress by the "push-forward" operation [19], $\sigma=J^{-1}\mathbf{FSF}T$. In our applications using ABAQUS, the updated Lagrangian formulation is adopted.

Objective Rate of Stress Tensor and Tangent Moduli

For FE implementation of user defined material models, the stress tensor and the tangent modulus tensor derived from the constitutive model need to be explicitly specified. In addition, to account for material rotation, an objective rate of the stress tensor is needed for the FE implementation [20]. Different forms of the tangent modulus tensor can be obtained in terms of different stress rates. Therefore, one should be cautious regarding which objective rate of a stress tensor should be used when developing a user material model.

In the paper by Miehe [17], the convected rate (also called the Oldroyd rate, or Lie-type derivative) of the Kirchhoff stress was used. The convected rate $L_{\upsilon}\tau$ of the Kirchhoff stress can be written as

$$L_{\upsilon}\boldsymbol{\tau}=\dot{\boldsymbol{\tau}}-\mathbf{L}\boldsymbol{\tau}-\boldsymbol{\tau}\mathbf{L}^{T}=\mathbb{C}^{\tau c}:\mathbf{D} \tag{2}$$

where the superposed dot denotes the material time derivative and $\mathbb{C}^{\tau c}$ is the tangent modulus tensor (or spatial elasticity tensor) for the convected rate of the Kirchhoff stress [19]. The rate-of-deformation tensor **D** and spin tensor **W** are the symmetric and antisymmetric parts of the spatial velocity gradient **L**, respectively. In the current treatment, we consider a different objective stress rate, $\overset{\nabla}{\boldsymbol{\tau}}$, the Jaumann rate of the Kirchhoff stress. The Jaumann rate, frequently used in the current finite element software and adopted by ABAQUS for continuum elements, can be expressed as

$$\overset{\nabla}{\boldsymbol{\tau}}=\dot{\boldsymbol{\tau}}-\mathbf{W}\boldsymbol{\tau}-\boldsymbol{\tau}\mathbf{W}^{T}=\mathbb{C}^{\tau J}:\mathbf{D} \tag{3}$$

where $\mathbb{C}^{\tau J}$ is the tangent modulus tensor for the Jaumann rate of the Kirchhoff stress. The relationship between $\mathbb{C}^{\tau c}$ and $\mathbb{C}^{\tau J}$ can be expressed in component form as

$$\mathbb{C}^{\tau J}_{ijkl}=\mathbb{C}^{\tau c}_{ijkl}+\delta_{ik}\tau_{jl}+\delta_{jl}\tau_{ik} \tag{4}$$

where δ_{ij}, the Kronecker delta, represents components of the rank 2 identity tensor.

Numerical Approximation of the Tangent Moduli

A numerical approximation of the tangent modulus tensor for the convected rate of Kirchhoff stress, $\mathbb{C}^{\tau c}$, was presented in the paper by Miehe [17]. Here, following a similar approach, we derive a numerical approximation for the tangent modulus tensor for the Jaumann rate of Kirchhoff stress, $\mathbb{C}^{\tau J}$. The approximation approach is based on the idea that by perturbing the deformation gradient on the linearized form of Eq. (3), the tangent moduli from the Jaumann rate of the Kirchhoff stress can be represented and approximated by a forward difference of the associated Kirchhoff stresses.

The linearized incremental form of Eq. (3) can be expressed as

$$\boldsymbol{\Delta\tau} - \boldsymbol{\Delta W\tau} - \boldsymbol{\tau\Delta W}^T = \mathbb{C}^{\tau J} : \boldsymbol{\Delta D} \tag{5}$$

where

$$\boldsymbol{\Delta W} = \frac{1}{2}(\boldsymbol{\Delta F F}^{-1} - (\boldsymbol{\Delta F F}^{-1})^T) \tag{6}$$

$$\boldsymbol{\Delta D} = \frac{1}{2}(\boldsymbol{\Delta F F}^{-1} + (\boldsymbol{\Delta F F}^{-1})^T) \tag{7}$$

To obtain the approximation of each of the components of $\mathbb{C}^{\tau J}$, a small perturbation to Eq. (5) is needed. The perturbation in the rate of deformation tensor, **ΔD**, has six independent components due to its symmetry properties. We denote $\boldsymbol{\Delta D}^{(ij)}$ as the perturbed **ΔD** produced by perturbing only its (*i*,*j*) component (no summation). Thus, the choice of (*ij*) would be (11) and (22), (33), (12), (13), and (23), and Eq. (7) can be rewritten for a perturbed condition as

$$\boldsymbol{\Delta D}^{(\mathrm{ij})} = \frac{1}{2}(\boldsymbol{\Delta F}^{(\mathrm{ij})}\mathbf{F}^{-1} + (\boldsymbol{\Delta F}^{(\mathrm{ij})}\mathbf{F}^{-1})^T) \tag{8}$$

where $\boldsymbol{\Delta F}^{(ij)}$ is the associated perturbation of the deformation gradient **F** produced by perturbing only its (*i*,*j*) component. Following Miehe [17], we now choose $\boldsymbol{\Delta F}^{(ij)}$ as

$$\boldsymbol{\Delta F}^{(\mathrm{ij})} = \frac{\varepsilon}{2}(e_i \otimes e_j\mathbf{F} + e_j \otimes e_i\mathbf{F}) \tag{9}$$

where ε is a small perturbation parameter and $\{e_i\}_{i=1,2,3}$denotes the basis vectors in the spatial description.

By inserting Eq. (9) into Eqs. (6) and (7), we obtain

$$\boldsymbol{\Delta W}^{(\mathrm{ij})} = \mathbf{0} \tag{10}$$

$$\boldsymbol{\Delta D}^{(\mathrm{ij})} = \frac{\varepsilon}{2}(e_i \otimes e_j + e_j \otimes e_i) \tag{11}$$

The perturbed deformation gradient $\mathbf{F}^{\wedge (ij)}$ can be expressed as

$$\hat{\mathbf{F}}^{(\mathrm{ij})}=\mathbf{F}+\Delta\mathbf{F}^{(\mathrm{ij})} \tag{12}$$

and $\Delta\boldsymbol{\tau}$ can be approximated by the forward difference of the perturbed and unperturbed Kirchhoff stresses,

$$\Delta\boldsymbol{\tau} \approx \boldsymbol{\tau}(\hat{\mathbf{F}}^{(\mathrm{ij})}) - \boldsymbol{\tau}(\mathbf{F}) \tag{13}$$

By inserting Eqs. (10), (11), and (13) into Eq. (5), we have

$$\boldsymbol{\tau}(\hat{\mathbf{F}}^{(\mathrm{ij})}) - \boldsymbol{\tau}(\mathbf{F}) \approx \mathbb{C}^{\tau J(\mathrm{ij})} : \frac{\varepsilon}{2}(e_i \otimes e_j + e_j \otimes e_i) \tag{14}$$

where $\mathbb{C}^{\tau J(ij)}$ represents the associated tangent moduli, or the components of the tangent modulus tensor $\mathbb{C}^{\tau J}$ obtained by the perturbation of $\Delta\mathbf{F}^{(ij)}$. By exploiting symmetry properties, Eq. (14) produces a concise form of the numerical approximation to the tangent moduli,

$$\mathbb{C}^{\tau J(\mathrm{ij})} \approx \frac{1}{\varepsilon}[\boldsymbol{\tau}(\hat{\mathbf{F}}^{(\mathrm{ij})}) - \boldsymbol{\tau}(\mathbf{F})] \tag{15}$$

The material Jacobian, $\mathbb{C}^{MJ}$, defined in ABAQUS, is

$$\mathbb{C}^{\mathrm{MJ}} = \frac{1}{J}\mathbb{C}^{\tau J} \tag{16}$$

Thus, we can rewrite Eq. (15) as

$$\mathbb{C}^{\mathrm{MJ(ij)}} \approx \frac{1}{J\varepsilon}[\boldsymbol{\tau}(\hat{\mathbf{F}}^{(\mathrm{ij})}) - \boldsymbol{\tau}(\mathbf{F})] \tag{17}$$

where $\mathbb{C}^{MJ(ij)}$ is the material Jacobian obtained by the perturbation of $\Delta\mathbf{F}^{(ij)}$. For hyperelastic materials, $\mathbb{C}^{MJ}$ possesses major symmetries and has only 21 independent components at each strain state. From Eq. (17) it can be seen that for each perturbation of $\Delta\mathbf{F}^{(ij)}$, six independent components of $\mathbb{C}^{MJ(ij)}$ can be determined. Thus there are 36 components of $\mathbb{C}^{MJ(ij)}$ that can be obtained after the six perturbations of $\Delta\mathbf{F}^{(ij)}$. These 36 components form a symmetric 6×6 matrix, and its 21 independent components furnish the $\mathbb{C}^{MJ(ij)}$ of a hyperelastic material.

To our knowledge, Eqs. (15) and (17) have not been reported before in the literature. As both Eq. (15) and Eq. (17) are material model independent, only a closed form equation for the Cauchy stress needs to be specified in coding a user material subroutine.

Validation of the Approximation Method

As an initial validation of the approximation method, we consider the neo-Hookean hyperelastic material model. For a finite element implementation, a penalty form of the neo-Hookean model can be expressed as

$$\psi = G(\bar{I}_1 - 3) + \frac{1}{D}(J-1)^2 \tag{18}$$

where G is the material constant describing the shear behavior of the material, D is the material constant that introduces the near incompressibility, and $\bar{I}_1 = \mathrm{tr}(\bar{\mathbf{C}})$ is the first strain invariant of the deviatoric right Cauchy–Green tensor $\bar{\mathbf{C}}$. In the limit as D approaches zero, the deformation behavior approaches that of a true incompressible neo-Hookean material.

The Cauchy stress σ derived from Eq. (18) can be expressed as

$$\sigma = \frac{2}{J} G \left(\bar{\mathbf{b}} - \frac{1}{3}\mathrm{tr}(\bar{\mathbf{b}})\mathbf{I} \right) + \frac{2}{D}(J-1)\mathbf{I} \tag{19}$$

Furthermore, the closed-form material Jacobian is given in component form as [21]

$$\begin{aligned} \mathbb{C}^{\mathrm{MJ}}_{ijkl} = & \frac{2}{J} G \left(\tfrac{1}{2}(\delta_{ik}\overline{b_{jl}} + \overline{b_{ik}}\delta_{jl} + \delta_{il}\overline{b_{jk}} + \overline{b_{il}}\delta_{jk}) - \tfrac{2}{3}(\delta_{ij}\overline{b_{kl}} + \overline{b_{ij}}\delta_{kl}) \right. \\ & \left. + \tfrac{2}{9}\delta_{ij}\delta_{kl}\overline{b_{mm}} + \tfrac{2}{D}(2J-1)\delta_{ij}\delta_{kl} \right) \end{aligned} \tag{20}$$

A single element implementation of the neo-Hookean model was used to evaluate the approximation method. The single element model consisted of a three-dimensional (3D), 20-node quadratic brick element with reduced integration (ABAQUS element type C3D20R) and dimensions of 1×1×1 mm^3. The material constants in Eq. (18) were set as G=80.0 kPa and D=2.0×10^{-4} kPa^{-1}. Twenty equal sized increments were used to apply 6.0 mm equibiaxial in-plane extensions with no constraint on out-of-plane deformation. Both Eq. (20) and Eq. (17) were coded in ABAQUS via user defined material subroutines (ABAQUS/UMAT). One simulation was performed using the exact material Jacobian given by Eq. (20), and five simulations were performed using the approximate material Jacobian given by Eq. (17) with various values of the perturbation parameter ε(1.0×10^{-4}, 1.0×10^{-6}, 1.0×10^{-8}, 1.0×10^{-10}, and 1.0×10^{-12}). Static simulations were performed, allowing for nonlinearity arising from both the constitutive law and the large geometric deformations, and the default convergence criteria set by ABAQUS was kept unchanged for all simulations.

As inaccurate tangent moduli will slow the convergence, the accuracy of the approximation method was evaluated by examining the number of iterations required to reach a convergent solution for each increment and the relative errors (REs) of the tangent moduli calculated by using Eq. (17) compared with those calculated using Eq. (20). Note that the closed-form solution of Eq. (20) always gives the most rapid convergence and thus requires the fewest numbers of iterations. Similarly, more accurate approximation methods will require fewer iterations to reach convergence. The RE is defined by the equation

$$\mathrm{RE} = \frac{(\text{value from Eq. (20)} - \text{approximte value from Eq. (17)})}{\text{value from Eq.(20)}}$$

For a 3D 20-node quadratic brick element with reduced integration, the element stiffness matrices are formed at eight integration points at each iteration. As the deformation in this example is homogeneous, moduli can be compared at a single integration point.

Application to Soft Tissue Modeling

In this second numerical example, we implemented a complex anisotropic constitutive model and performed FE simulations of artery inflation utilizing the approximation approach of Eq. (17) as a sample application to a more complex situation without a convenient analytical solution. In order to describe the mechanics of fibrillar soft tissues, formulations motivated by the theory of fiber-reinforced composites [22] are often employed. In particular, the fiber-reinforced hyperelastic material model proposed by Holzapfel and Gasser [6,23] has been shown to accurately capture the behavior of blood vessel inflation under internal pressurization. In that model, the blood vessel is idealized as a cylindrical body composed of a matrix material with two families of imbedded fibers, each of which is unidirectional with a preferred direction. The fiber directions can be mathematically described using two unit vectors m_0 and n_0. The strain invariants $\bar{I}_4$ and $\bar{I}_6$ of $\bar{\mathbf{C}}$, which are given by $\bar{I}_4 = m_0 \cdot \bar{\mathbf{C}} m_0$ and $\bar{I}_6 = n_0 \cdot \bar{\mathbf{C}} n_0$, can be used to describe the properties of the fiber families. $\bar{I}_4$ and $\bar{I}_6$ are equal to the squares of the stretches in the fiber directions m_0 and n_0, respectively.

The strain-energy function ψ of Holzapfel's model can be approximated as [6]

$$\psi = G(\bar{I}_1 - 3) + \frac{k_1}{2k_2}\left(\left(\exp\left[k_2(\bar{I}_4 - 1)^2\right] - 1\right) + \left(\exp\left[k_2(\bar{I}_6 - 1)^2\right] - 1\right)\right) + \frac{1}{D}(J-1)^2 \tag{21}$$

where G, k_1, k_2, and D are material constants. G and D have the same physical meanings as those in Eq. (18), while k_1 is a positive material constant with the dimensions of stress and k_2 is a dimensionless parameter. As in the neo-Hookean example, we introduce the incompressibility constraint through a penalty term, with near incompressibility enforced as D approaches zero.

The symmetric second Piola–Kirchhoff stress $\mathbf{S}$ can be obtained by the derivatives of the strain-energy function ψ of Eq. (21) with respect to the right Cauchy–Green tensor $\mathbf{C}$. The insertion of Eq. (21) into Eq. (1) gives the representation

$$\mathbf{S} = J^{-2/3}\left(\mathbb{I} - \frac{1}{3}\mathbf{C}^{-1} \otimes \mathbf{C}\right) : 2(G\mathbf{I}) + 2(\bar{\psi}_4 m_0 \otimes m_0 + \bar{\psi}_6 n_0 \otimes n_0) + \frac{2J}{D}(J-1)\mathbf{C}^{-1} \tag{22}$$

where

$$\bar{\psi}_4 = (\bar{I}_4 - 1)k_1 \exp\left[k_2(\bar{I}_4 - 1)^2\right] \tag{23}$$

$$\bar{\psi}_6 = (\bar{I}_6 - 1)k_1 \exp\left[k_2(\bar{I}_6 - 1)^2\right] \tag{24}$$

$\mathbb{I}$ is the fourth order unit tensor with components $(\mathbb{I})_{abcd} = (\delta_{ac}\delta_{bd} + \delta_{ab}\delta_{cd})/2$. The corresponding Cauchy stress $\boldsymbol{\sigma}$ can be easily obtained by using the push-forward operation [19], and the associated Kirchhoff stress $\boldsymbol{\tau}$ can be obtained by utilizing Eq. (1).

The closed-form elasticity tensor in the material or spatial description can be determined following the procedure described by Holzapfel [19]. For an ABAQUS implementation, a proper transformation following Eq. (4) should be adopted to obtain the correct tangent moduli.

Zulliger et al. [16] utilized this model to describe experimental pressure-diameter data generated by inflation of rat carotid arteries. From the experimental sample geometry described by Zulliger et al. [16], we constructed a FE model of rat carotid artery segment with an inner diameter of 0.3 mm, an outer diameter of 0.4 mm, and length of 0.05 mm (Fig. 1). The model consisted of 10100 nodes and 1800 3D continuum brick elements (ABAQUS element type C3D20R), with six layers of elements through the wall and three layers of elements along the longitudinal axis. Axial deformation was constrained at both ends, and radial expansion was allowed. Based on the data presented by Zulliger et al. [16], material constants were assigned as G=22.12 kPa, k_1=0.206 kPa, k_2=1.465, and D=2.0×10^4 kPa^{-1}, and the preferred collagen fiber orientation was at ±39.76 deg with respect to the vessel circumferential direction. Based on the results of the single element validation, the perturbation parameter was set as ε=1.0×10^{-8}. A constant pressure of 25 kPa was uniformly applied to the inner surface of the artery, and the inner and outer radii were reported for each pressure increment. Automatic incrementation control was specified such that ABAQUS could automatically adjust the size of the increments to solve the nonlinear problem efficiently. The only difference from the neo-Hookean model in the ABAQUS/UMAT subroutine was the constitutive definition of the stress.

To investigate the influence of the perturbation parameter ε on model convergence, simulations were conducted with ε prescribed as 1.0×10^{-4}, 1.0×10^{-6}, 1.0×10^{-10}, and 1.0×10^{-12}, but with all other parameters held constant. In addition, the influence of the penalty term D on the model predictions was also explored with D prescribed as 2.0×10^{-2}, 2.0×10^{-3}, 2.0×10^4, and 2.0 ×10^{-5} kPa^{-1} but with all other parameters held constant.

Results

Validation of the Approximation Method

For the single element model, the numbers of iterations required to reach convergence at each increment were similar for all six simulations (Table 1). The total number of equilibrium iterations over the 20 increments was 47, using the analytical expression for the tangent moduli given by Eq. (20), while totals of 49, 47, 47, 47, and 50 iterations were required using the approximate expression given by Eq. (17) with ε=1.0×10^{-4}, 1.0×10^{-6}, 1.0×10^{-8}, 1.0×10^{-10}, and 1.0×10^{-12}, respectively. Although there were slight degradations in efficiency for the highest and lowest values of the perturbation parameter, the overall efficiency of the approximation method was close to that of the closed-form solution for this example.

For a detailed comparison of the tangent modulus values calculated using Eq. (20) and Eq. (17), we evaluated the relative errors in nine major components of the tangent moduli at the second loading increment (Table 2), which represented the biggest discrepancy in convergence in the simulation. The tangent moduli obtained from the approximate method demonstrated close matches to those obtained from the closed-form formulation for all simulations. The relative errors are on the order of magnitudes of, for example, 1.0×10^{-3}–1.0×10^{-7} for ε=1.0×10^{-4} and 1.0 ×10^{-6}–1.0×10^{-10} for ε=1.0×10^{-8}. Note that when ε=1.0×10^{-8}, the tangent moduli obtained using Eq. (17) showed the closest match to those obtained using Eq. (20).

Artery Inflation Simulations

Using the approximation approach of Eq. (17), we were able to quickly implement the complex material model of Eq. (21) in FE simulations without an explicit development of a closed-form solution for the tangent stiffness matrix, thus eliminating the associated coding. With ABAQUS default convergence criteria, the simulation finished in 25 increments without encountering convergence issues. The pressure-radius data output from the simulation closely matched the experimental data reported in Zulliger et al. [16], as shown in Fig. 1.

For the five simulations using Eq. (17), with ε varied from 1.0×10^{-4} to 1.0×10^{-12}, the number of equilibrium iterations required to reach convergence at each increment was similar (Table 3) with a slight increase in iterations when $\varepsilon=1.0\times10^{-12}$. The total number of equilibrium iterations during the 25 increments was 52 when using Eq. (17) with $\varepsilon=\times10^{-4}$, 1.0×10^{-6}, 1.0×10^{-8}, 1.0×10^{-10}, and 58 when using Eq. (17) with $\varepsilon=1.0\times10^{-12}$.

The initial and deformed geometries of the artery segment and a close-up view of the transmural stress distribution are illustrated in Fig. 2. To examine the transmural stress distribution under different pressure loadings, transmural maximum principal stress distributions across the artery wall were plotted for five increments, corresponding to pressures of 4.92 kPa, 11.08 kPa, 16.62 kPa, 19.39 kPa, and 25.00 kPa (Fig. 3). At low pressure (for example, at 4.92 kPa), the transmural stresses were relatively uniform. However, at higher pressures (for example, at 25 kPa), the stress at the inner wall (intimal-media layer) was much higher than that of the outer wall (adventitial layer). It should be noted that this simulation did not account for physiologic residual stresses in the artery wall, so this simulation likely overpredicted the actual inner wall stress. Such a treatment is beyond the scope of this study, but incorporation of residual stresses will be important in practical applications of this approach to investigations of artery mechanical responses.

As shown in Fig. 4, the choice of the penalty parameter D does impact the simulation results. When choosing $D=2.0\times10^{-2}$, the simulated vessel wall was more compliant than the actual vessel (experimental data). Reducing the value of D caused the compliance of the simulated vessel wall to converge to the experimental data, with negligible difference between $D=2.0\times10^{-4}$ and $D=2.0\times10^{-5}$.

Discussion

Finite element simulations using sophisticated soft tissue models have been rather limited in general purpose commercial FE codes such as ABAQUS and ANSYS. Currently, ABAQUS and ANSYS, as well as other commercial FE codes, only provide support for several isotropic hyperelastic models such as Mooney–Rivlin and Ogden models. The implementation of a nonlinear anisotropic hyperelastic model requires the development of a user material subroutine. In this paper, we present a method that can facilitate FE implementation of sophisticated soft tissue models. Using the fiber-reinforced material model developed by Holzapfel and Gasser [6] as a numerical example, we demonstrated the feasibility and simplicity of using the approach to perform a FE simulation involving a complex tissue model.

Selection of Perturbation Parameter ε

The approximation method proposed in this paper is based on a perturbation of the deformation gradient such that the tangent moduli from the Jaumann rate of the Kirchhoff stress can be approximated by a forward difference of the associated Kirchhoff stresses. The selection of an appropriate value of the perturbation parameter ε is therefore important. As indicated in Table 1 and Table 3, choosing a perturbation parameter that is too large (in this case, $\varepsilon=1.0\times10^{-4}$) or too small (in this case, $\varepsilon=1.0\times10^{-12}$) results in an increase in the number of iterations required to finish the simulations. When the perturbation parameter is too large, the inherent error in the approximation increases. Conversely, when the perturbation parameter becomes small, issues related to computer precision can introduce errors despite a theoretical improvement in the approximation accuracy. When using a double precision FE code, ε cannot be less than 10^{-16}. Even though no difference between using $\varepsilon=1.0\times10^{-6}$, 1.0×10^{-8}, and 1.0×10^{-10} was shown in Table 1 and Table 3, a detailed examination of the values of some components of the tangent moduli in Table 2 revealed that when using $\varepsilon=1.0\times10^{-8}$ the relative errors were smallest in all selections of ε. Thus, in our applications, 1.0×10^{-8} appeared to be an appropriate value for the approximation method. We suggest this perturbation parameter as a starting point, but

an appropriate range of perturbation parameters should be determined for any new constitutive model (e.g., through single element analyses as in our first example).

Artery Inflation Simulations

In a simulation of artery inflation using a sophisticated material model, a converged finite element solution is often difficult to obtain, especially at a high pressure region. In this artery inflation example, the high pressure region was from 15 kPa to 25 kPa. In this region, the typical strain-stiffening tissue behavior, which is caused by stiffening of collagen fibers, results in a limited increase in artery radius at high pressures.

For an implicit finite element simulation using Newton's method to resolve the equilibrium equations iteratively, it was demonstrated [24] that numerical solutions of highly nonlinear tissue behaviors require the tangent stiffness matrix to be well conditioned. Such well-conditioned matrix properties include convexity and a low condition number. The approximate solutions of the tangent moduli should be close to the closed-form solution to ensure the efficacy of using Newton's method to achieve a rapid convergence and also to preserve the well-conditioned matrix properties of the closed-form solution.

We perturbed ε by orders of magnitude between 1.0×10^{-4} and 1.0×10^{-12}, and converged solutions with similar convergence rates were achieved for all conditions, illustrating the robustness and efficiency of the approximation approach.

Summary

In this study, a numerical approximation method for the determination of tangent moduli for general hyperelastic material models is presented. The approach to estimating tangent moduli is material model independent; i.e., once the approximation method is coded in a user material subroutine, it can be used for other hyperelastic material models with no modification and merely requires coding of a correct stress tensor. Moreover, the approximation is mathematically concise and can thus be implemented in a straightforward manner. Since the approach is developed on a widely utilized, commercially available FE platform ABAQUS, it is hoped that it will greatly facilitate the incorporation of nonlinear anisotropic soft tissue models into FE simulations.

Acknowledgment

This work was funded in part by NIH Grant No. 5R01HL071136.

References

1. Nielsen PM, Hunter PJ, Smaill BH. Biaxial Testing of Membrane Biomaterials: Testing Equipment and Procedures. ASME J. Biomech. Eng 1991;113(3):295–300.
2. Kyriacou SK, Shah AD, Humphrey JD. Inverse Finite Element Characterization of Nonlinear Hyperelastic Membranes. ASME J. Appl. Mech 1997;64:257–262.
3. Humphrey JD, Strumpf RK, Yin FC. Determination of a Constitutive Relation for Passive Myocardium: II. Parameter Estimation. ASME J. Biomech. Eng 1990;112(3):340–346.
4. Weiss JA, Maker BN, Govindjee S. Finite Element Implementation of Incompressible, Transversely Isotropic Hyperelasticity. Comput. Methods Appl. Mech. Eng 1996;135:107–128.
5. Gardiner JC, Weiss JA. Simple Shear Testing of Parallel-Fibered Planar Soft Tissues. ASME J. Biomech. Eng 2001;123(2):170–175.
6. Holzapfel GA, Gasser TC. A New Constitutive Framework for Arterial Wall Mechanics and a Comparative Study of Material Models. J. Elast 2000;61:1–48.
7. Tong P, Fung YC. The Stress-Strain Relationship for the Skin. J. Biomech 1976;9(10):649–657. [PubMed: 965417]

8. Chew PH, Yin FC, Zeger SL. Biaxial Stress-Strain Properties of Canine Pericardium. J. Mol. Cell. Cardiol 1986;18(6):567–578. [PubMed: 3735439]
9. Fung YC, Liu SQ, Zhou JB. Remodeling of the Constitutive Equation While a Blood Vessel Remodels Itself Under Stress. ASME J. Biomech. Eng 1993;115(4B):453–459.
10. Criscione JC, Sacks MS, Hunter WC. Experimentally Tractable, Pseudo-Elastic Constitutive Law for Biomembranes: I. Theory. ASME J. Biomech. Eng 2003;125(1):94–99.
11. Criscione JC, Sacks MS, Hunter WC. Experimentally Tractable, Pseudo-Elastic Constitutive Law for Biomembranes: II. Application. ASME J. Biomech. Eng 2003;125(1):100–105.
12. Sun W, Sacks MS, Sellaro TL, Slaughter WS, Scott MJ. Biaxial Mechanical Response of Bioprosthetic Heart Valve Biomaterials to High In-Plane Shear. ASME J. Biomech. Eng 2003;125:372–380.
13. Lanir Y. Plausibility of Structural Constitutive-Equations for Isotropic Soft-Tissues in Finite Static Deformations. Trans. ASME, J. Appl. Mech 1994;61(3):695–702.
14. Billiar KL, Sacks MS. Biaxial Mechanical Properties of the Native and Glutaraldehyde-Treated Aortic Valve Cusp: Part II—A Structural Constitutive Model. ASME J. Biomech. Eng 2000;122(4):327–335.
15. Sacks MS. Incorporation of Experimentally-Derived Fiber Orientation Into a Structural Constitutive Model for Planar Collagenous Tissues. ASME J. Biomech. Eng 2003;125(2):280–287.
16. Zulliger MA, Fridez P, Hayashi K, Stergiopulos N. A Strain Energy Function for Arteries Accounting for Wall Composition and Structure. J. Biomech 2004;37(7):989–1000. [PubMed: 15165869]
17. Miehe C. Numerical Computation of Algorithmic (Consistent) Tangent Moduli in Large-Strain Computational Inelasticity. Comput. Methods Appl. Mech. Eng 1996;134:223–240.
18. Bathe, KJ. Finite Elements Proceedures. Englewood Cliffs, NJ: Prentice-Hall; 1995.
19. Holzapfel, GA. Nonlinear Solid Mechanics: A Continuum Approach for Engineering. Chichester: Wiley; 2000.
20. Belytschko, T.; Liu, WK.; Moran, B. Nonlinear Finite Elements for Continua and Structures. Chichester: Wiley; 2000.
21. ABAQUS, 1.1.14 Analysis of an Automotive Boot Seal. ABAQUS Example Problems Manual. 2006ABAQUS 6.6 Documentation.
22. Spencer, A. Deformations of Fibre-Reinforced Materials. Glasgow: Oxford University Press; 1972.
23. Holzapfel GA, Gasser TC. A Viscoelastic Model for Fiber-Reinforced Composites at Finite Strains: Continuum Basis, Computational Aspects and Applications. Comput. Methods Appl. Mech. Eng 2001;190(34):4379–4403.
24. Sun W, Sacks MS. Finite Element Implementation of a Fung Elastic Model for Planar Anisotropic Biological Materials. Biomechanics and Modeling in Mechanobiology 2005;4(2–3):190–199. [PubMed: 16075264]

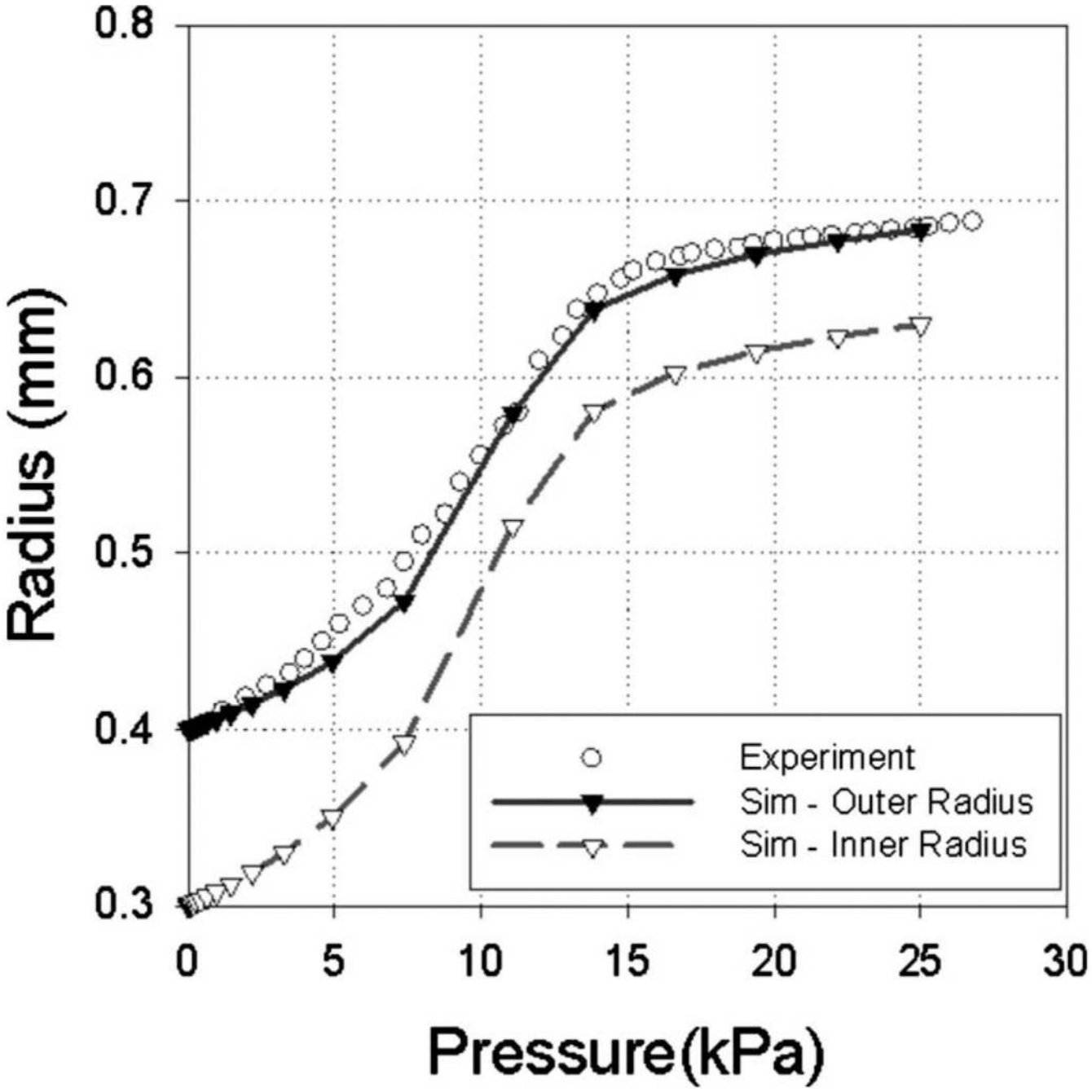

Fig. 1.

With the material constants G=44.24 kPa, k_1 =0.206 kPa, k_2=1.465, and D=2.0×10^{-4} kPa^{-1} and fiber orientations of ±39.76 deg, pressure-radius results from the FE model were compared with experimental data, adapted from Fig. 7 of Zulliger et al. [16]

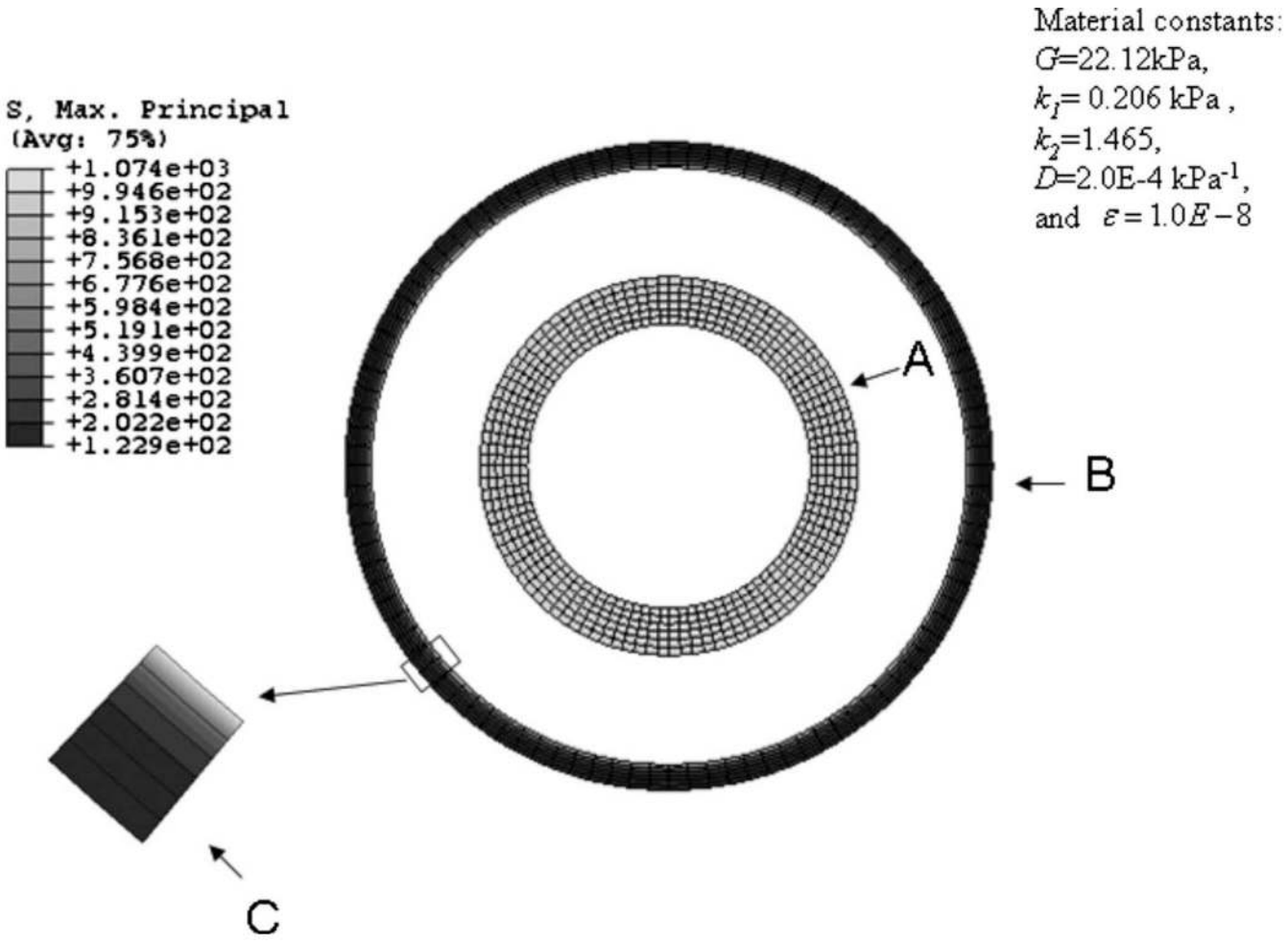

Fig. 2.

The FE model for a rat carotid artery segment, (A) before deformation, (B) deformed geometry after a 25 kPa inner pressure in a maximum principal stress contour plot, (C) a radial segment of the FE model showing the stress distribution across the artery wall thickness. The FE model geometry, material constants, and loading conditions were adopted from Zulliger et al. [16].

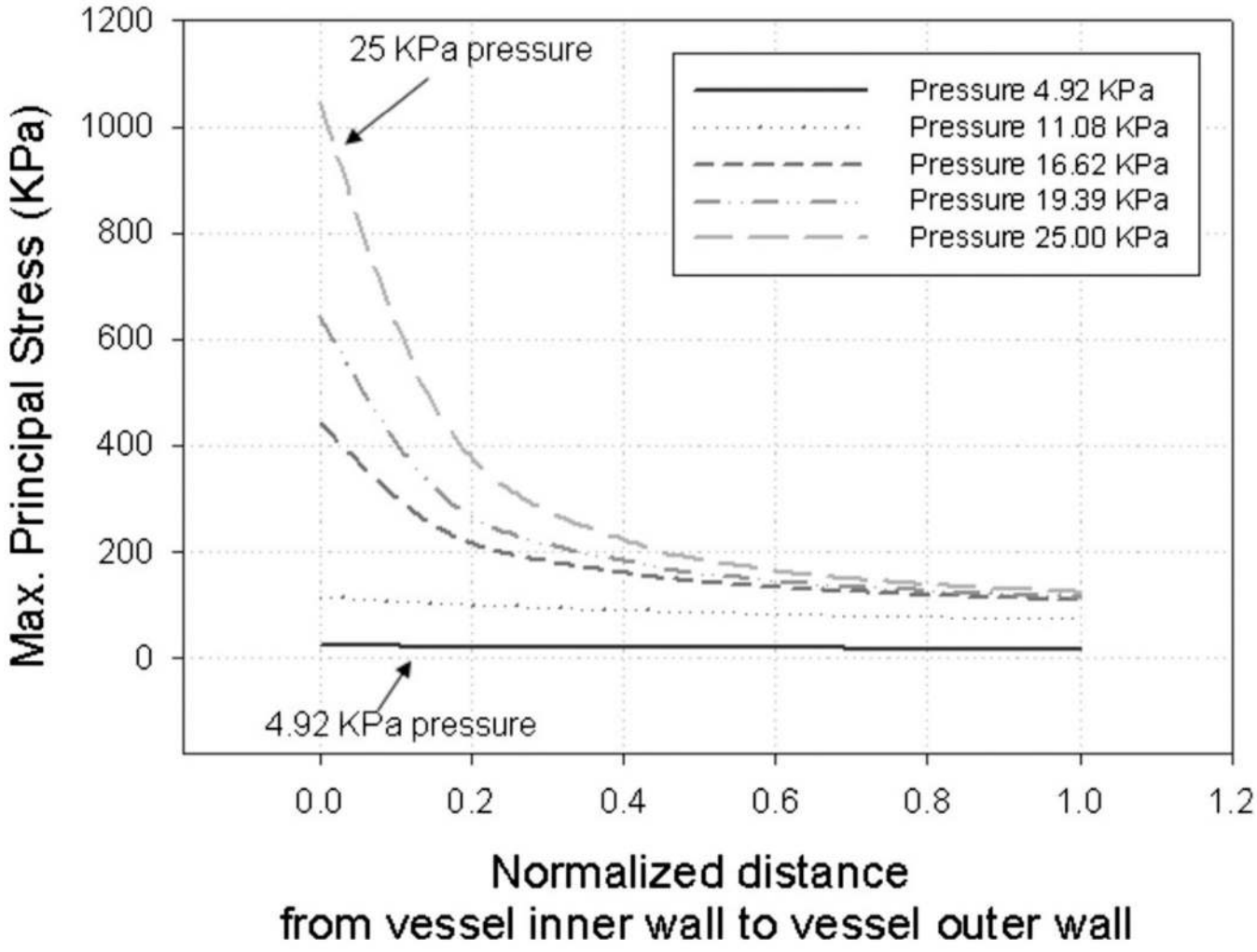

Fig. 3.
Maximum principal stress across the artery wall thickness under different static pressures

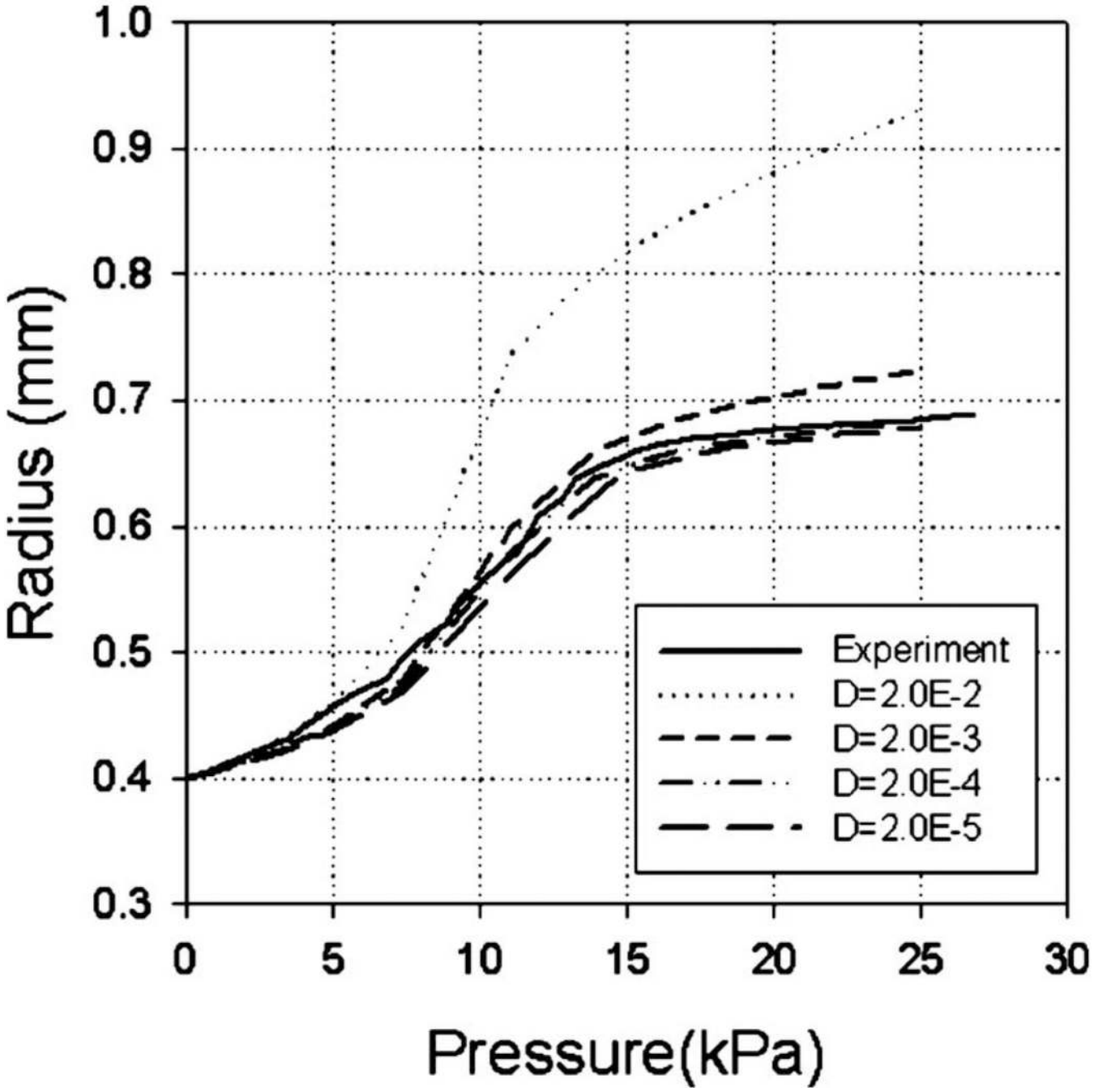

Fig. 4.

Pressure-radius plots of simulated artery inflations with the variation in incompressibility control parameter D with values of 2.0×10^{-2}, 2.0×10^{-3}, 2.0×10^{-4}, and 2.0×10^{-5}

Table 1

The number of equilibrium iterations for each increment step during an equibiaxial extension of a single element model using the neo-Hookean material model Eq. (18). The tangent moduli utilized in the simulations were obtained from the closed-form solution of Eq. (20). and the approximation method of Eq. (17). with the perturbation parameter $\varepsilon = 1.0\times10^{-04}$, 1.0×10^{-6}, 1.0×10^{-8}, 1.0×10^{-10} and 1.0×10^{-12}.

Increment steps	Equilibrium iterations					
		Eq. (17)				
	Eq. (20)	$\varepsilon=1.0\times10^{-4}$	$\varepsilon=1.0\times10^{-6}$	$\varepsilon=1.0\times10^{-8}$	$\varepsilon=1.0\times10^{-10}$	$\varepsilon=1.0\times10^{-12}$
1	3	3	3	3	3	3
2	4	5	4	4	4	7
3–6	3	3	3	3	3	3
7	2	2	2	2	2	2
8	2	3	2	2	2	2
9–20	2	2	2	2	2	2
Total	47	49	47	47	47	50

J Biomech Eng. Author manuscript; available in PMC 2009 August 11.

Table 2

Nine components of the tangent moduli from integration point 1 at increment 2 were listed for Eq. (20). and the associated relative errors of Eq. (17). with the perturbation value $\varepsilon=1.0\times10^{-4}$, 1.0×10^{-6}, 1.0×10^{-8}, 1.0×10^{-10} and 1.0×10^{-12}

Tangent stiffness modulus	Eq. (20)	Relative error (RE) of using Eq. (17)				
		$\varepsilon=1.0\times10^{-4}$	$\varepsilon=1.0\times10^{-6}$	$\varepsilon=1.0\times10^{-8}$	$\varepsilon=1.0\times10^{-10}$	$\varepsilon=1.0\times10^{-12}$
C1111	$1.626818410393820\times10^{3}$	-2.572×10^{-4}	-2.574×10^{-6}	-6.852×10^{-8}	1.308×10^{-6}	-4.032×10^{-4}
C2222	$1.626818410393830\times10^{3}$	-2.285×10^{-4}	-2.287×10^{-6}	-1.388×10^{-8}	1.308×10^{-6}	-4.032×10^{-4}
C3333	$8.053775504572980\times10^{2}$	-4.101×10^{-4}	-4.106×10^{-6}	-2.055×10^{-7}	-1.029×10^{-5}	1.048×10^{-4}
C1212	$1.251687271447620\times10^{3}$	$-2.827\ 10^{-5}$	-2.821×10^{-7}	1.154×10^{-9}	-5.538×10^{-7}	1.207×10^{-4}
C1313	$6.356066264952270\times10^{2}$	-5.518×10^{-5}	-5.501×10^{-7}	-7.013×10^{-10}	-4.493×10^{-7}	9.588×10^{-5}
C2323	$6.356066264952310\times10^{2}$	-1.091×10^{-7}	-1.630×10^{-9}	2.955×10^{-9}	-6.315×10^{-7}	1.400×10^{-4}
C1122	$-8.765561325014270\times10^{2}$	4.176×10^{-4}	4.181×10^{-6}	1.401×10^{-7}	-4.280×10^{-6}	1.191×10^{-3}
C1133	$-5.511527256489250\times10^{1}$	6.401×10^{-3}	6.408×10^{-5}	2.860×10^{-6}	-2.571×10^{-4}	1.625×10^{-2}
C2233	$-5.511527256489800\times10^{1}$	7.248×10^{-3}	7.251×10^{-5}	1.247×10^{-6}	6.550×10^{-5}	1.254×10^{-4}

Table 3

The number of equilibrium iterations for each increment step during artery inflation simulations using the Holzapfel's model (Eq. (21)). The tangent moduli utilized in the simulations were obtained from the approximation method of Eq. (17). with the perturbation parameter $\varepsilon=1.0\times10^{-4}$, 1.0×10^{-6}, 1.0×10^{-8}, 1.0×10^{-10}, and 1.0×10^{-12}

Increment steps	Equilibrium iterations				
	Eq. (17)				
	$\varepsilon=1.0\times10^{-4}$	$\varepsilon=1.0\times10^{-6}$	$\varepsilon=1.0\times10^{-8}$	$\varepsilon=1.0\times10^{-10}$	$\varepsilon=1.0\times10^{-12}$
1, 2	1	1	1	1	1
3, 4	1	1	1	1	2
5, 6	2	2	2	2	2
7, 8	1	1	1	1	2
9–13	1	1	1	1	1
14	1	1	1	1	2
15–17	2	2	2	2	2
18, 19	3	3	3	3	3
20	4	4	4	4	4
21, 22	6	6	6	6	6
23	3	3	3	3	4
24	3	3	3	3	3
25	2	2	2	2	2
Total	52	52	52	52	58